Realizing and Detecting the Quantum Hall Effect without Landau Levels by Using Ultracold Atoms

L. B. Shao,[1,2,3] Shi-Liang Zhu,[1,*] L. Sheng,[2] D. Y. Xing,[2] and Z. D. Wang[3]

[1]*Institute for Condensed Matter Physics and Department of Physics, South China Normal University, Guangzhou, China*
[2]*National Laboratory of Solid State Microstructure and Department of Physics, Nanjing University, Nanjing, China*
[3]*Department of Physics and Center of Theoretical and Computational Physics, The University of Hong Kong,
Pokfulam Road, Hong Kong, China*

We design an ingenious scheme to realize Haldane's quantum Hall model without Landau levels by using ultracold atoms trapped in an optical lattice. Three standing-wave laser beams are used to construct a wanted honeycomb lattice, where different on site energies in two sublattices required in the model can be implemented through tuning the phase of one laser beam. The staggered magnetic field is generated from the light-induced Berry phase. Moreover, we establish a relation between the Hall conductivity and the atomic density, enabling us to detect the Chern number with the typical density-profile-measurement technique.

The quantum Hall effect (QHE) [1] in two-dimensional electron systems is one of the most peculiar quantum-mechanical phenomena observed in nature. The QHE is usually associated with a uniform external magnetic field, which splits the electron energy spectrum into discrete Landau levels (LLs). When the Fermi energy lies in the gap between two LLs, the Hall conductivity in units e^2/h is accurately quantized to an integer. The precise quantization of the Hall conductivity was explained by Laughlin [2] based upon a gauge invariance argument, which is fundamental to the picture of edge states proposed by Halperin [3]. On the other hand, Thouless, Kohmoto, Nightingale, and Nijs (TKNN) [4] interpreted the Hall conductivity as the topological Chern number of the $U(1)$ bundle over the magnetic Brillouin zone of the bulk states.

Twenty years ago, Haldane showed in principle that a QHE may also result from breaking of time-reversal symmetry without any net magnetic flux through a unit cell of a periodic two-dimensional (2D) system [5]. In his work, Haldane constructed a tight-binding model on a honeycomb lattice including a complex second nearest-neighbor hopping integral. The honeycomb lattice consists of two triangular sublattices $\bar{A}$ and $\bar{B}$ with different on site energies M and $-M$, as shown in Fig. 1(a). A periodic vector potential $\mathbf{A}(\mathbf{r})$ is applied to the lattice, given that the total magnetic flux through each unit cell vanishes, i.e., the first-neighbor hopping integral t is unaffected. The second-neighbor hopping integral t' acquires a Peierls phase factor $\exp(ie \int \mathbf{A} \cdot d\mathbf{r}/\hbar)$, where the integration is along the hopping path. The Hamiltonian of the model is written as

$$H = \sum_{\langle l,j \rangle}(ta_l^\dagger b_j + \text{H.c.}) + \sum_j M(a_j^\dagger a_j - b_j^\dagger b_j)$$
$$+ \sum_{\langle\langle l,j \rangle\rangle} t' e^{i\varphi_{jl}}(a_l^\dagger a_j + b_l^\dagger b_j), \qquad (1)$$

where a_i and b_i are the annihilation operators on site R_i in sublattices $\bar{A}$ and $\bar{B}$, respectively. φ_{jl} is the accumulated Peierls phase from site j to its second neighbor l, which is assumed to take the form $\varphi_{jl} = \pm\varphi$. The hopping directions for which $\varphi_{jl} = +\varphi$ are shown in Fig. 1(a). The most interesting and unique feature of the model lies in that the phase of the system can be changed from a normal insulator to a Chern insulator by the simulation of parity anomaly [5–11]. However, it is extremely hard to realize the Haldane's model experimentally in ordinary condensed matter systems because of the unusual staggered magnetic flux assumed in the model.

On the other hand, the technology of ultracold atoms in an optical lattice provides a perspective approach to explore rich fundamental phenomena of condensed matter physics [12–14]. In particular, how to realize the QHE with cold atoms has attracted considerable interest [15–19]. Nevertheless, the atomic QHE has not been observed yet, mainly due to challenges in both the realization and detection of the atomic Hall effects. Although an effective magnetic field for neutral atoms can be simulated either by rotating the atoms [20] or by laser-induced Berry phases [21–24], the strong magnetic field region required for QHE has not been reached yet in experiments. For the rotating method, the system is close to the point at which the centrifugal potential cancels the external harmonic trap, and the atoms may fly apart at the rotation speed required by QHE [16,19]. For the laser-induced Berry phase approach, the cold atoms moving in a spatially varying laser field feel an effective gauge potential [21–24], but the region of the strong uniform field is rather small for two typical counterpropagating Gaussian laser beams. In addition, the detection method for cold atoms is very different from that for condensed matter systems; especially, the widely used technique for QHE based on the transport
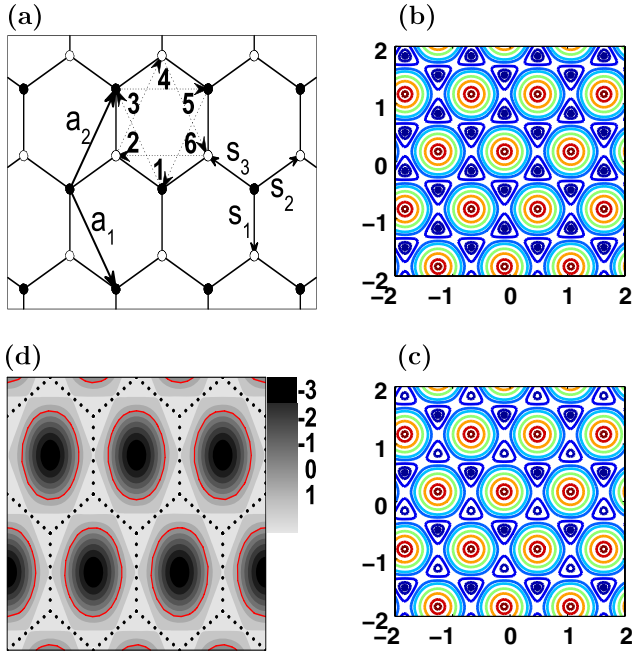
(a)

(b)

(d)

(c)

FIG. 1 (color online). (a) Illustration of the Honeycomb lattice structure of graphene, where open and solid circles represent sites in sublattices $\bar{A}$ and $\bar{B}$. $\mathbf{a}_1 = (\frac{1}{2}a, -\frac{\sqrt{3}}{2}a)$, $\mathbf{a}_2 = (\frac{1}{2}a, \frac{\sqrt{3}}{2}a)$ are the unit vectors of the underlying triangular sublattice. s_1, s_2, and s_3 are three vectors pointing from a $\bar{B}$ site to its three nearest-neighbor sites. (b) and (c) show the contours of the potential V for $\chi = 2\pi/3$ and $\chi = 39\pi/60$, respectively. The vertical (horizontal) axis represents yk_0^L/π (xk_0^L/π). (d) Contours of the magnetic field defined by Eq. (2).

measurements is not workable for atomic QHE. In this Letter, we design an ingenious scheme to realize the Haldane's quantum Hall model without LLs by using ultra-cold atoms trapped in an optical lattice. We work out a distinct method to construct the honeycomb lattices that have different on site energies by three standing-wave laser beams. Although it is still hard to achieve a strong homo-genous magnetic field required by the conventional QHE in atomic system, we may evade this bottleneck since LLs are not necessary in this unconventional QHE. We elaborate that the staggered magnetic field, which is hard to generate in condensed matter systems, may be rather easy to set up by other three standing-wave laser beams. In this scenario, different on site energies in two sublattices can be easily adjusted through tuning the phase of one of the laser beams, and thus the whole phase diagram [5] including the exotic topological phase transition predicted by Haldane may be revealed experimentally. Furthermore, based on $(2 + 1)$-dimensional relativistic quantum me-chanics calculations, we establish a direct relationship between the Hall conductivity and the equilibrium atomic density, such that the famous topological Chern number may be experimentally detected with the standard density profile measurement used in atomic systems [12].

Let us first consider single component fermionic atoms (e.g., ^{40}K, ^{6}Li, etc.) in a 2D honeycomb lattice [14,25],

which can be realized by three detuned laser beams. A detuned standing-wave laser beam will create a potential in the form $V_0 \sin^2(\mathbf{k}_0^L \cdot \mathbf{r})$, where V_0 is the potential ampli-tude and $\mathbf{k}_0^L$ is the wave vector of the laser. To generate the honeycomb lattice with different on site energies in sub-lattices $\bar{A}$ and $\bar{B}$, the three laser beams with the same wave length but different polarizations are applied along three different directions: $\mathbf{e}_y$ and $\frac{\sqrt{3}}{2}\mathbf{e}_x \pm \frac{1}{2}\mathbf{e}_y$, respectively. The potential is thus given by $V = V_0[\sin^2(\alpha_+ + \frac{\pi}{2}) + \sin^2(yk_0^L + \frac{\pi}{3}) + \sin^2(\alpha_- - \frac{\chi}{2})]$, where $\alpha_\pm = \sqrt{3}xk_0^L/2 \pm yk_0^L/2$. The potential contours are plotted in Fig. 1(b) and 1(c). Under these conditions, atoms are trapped at the minima of the potential, forming a honeycomb lattice. An amazing feature here is that the different site energies of sublattices $\bar{A}$ and $\bar{B}$ are controllable by the phase of laser beam χ. For instance, we get exactly the honeycomb lattice with the same on site energies ($M = 0$) for $\chi = \frac{2}{3}\pi$, as shown in Fig. 1(b), while the two sublattices have different on site energies ($M \neq 0$) for $\chi \neq \frac{2\pi}{3}$.

Now, we elaborate how to simulate the staggered mag-netic field in the Haldane's model. Since the net flux per unit cell vanishes, the vector potential applied to the lattice must be periodic. Such magnetic fields can be created by Berry phase induced from two opposite-travelling standing-wave laser beams [22]. For the two laser beams with Rabbi frequencies $\Omega_1 = \Omega_0 \sin(yk_2^L + \frac{\pi}{4})e^{ixk_1^L}$ and $\Omega_2 = \Omega_0 \cos(yk_2^L + \frac{\pi}{4})e^{-ixk_1^L}$, the effective gauge potential is generated as $\mathbf{A}_1(\mathbf{r}) = \hbar k_1^L \sin(2yk_2^L)\mathbf{e}_x$ [22]. Here, $k_1^L = k^L \cos\theta$ and $k_2^L = k^L \sin\theta$ with k^L the wave vector of the laser and θ the angle between the wave vector and the $\mathbf{e}_x$ axis. We emphasize that the choice of wave vector k_2^L of the laser beams must be a multiple of $\frac{2\sqrt{3}\pi}{3a}$ in order to be commensurate with the optical lattice. We take $k_2^L = \frac{2\sqrt{3}\pi}{3a}$. The Peierls phases for the nearest-neighbor hopping in Fig. 1(a) are $\varphi_{12} = \varphi_{61} = -\varphi_{34} = -\varphi_{45} = \varphi_0$ and $\varphi_{23} = \varphi_{56} = 0$. For the next-nearest-neighbor hopping integrals, which are integrated on a period of the vector potential, the corresponding accumulated phases are $\varphi_{13} = \varphi_{24} = \varphi_{46} = \varphi_{15} = 0$, and $\varphi_{35} = \varphi_{62} = \varphi$, where $\varphi = k_1^L a \sin\frac{ak_2^L}{\sqrt{3}}$. Since the lattice has the symmetry of point group C_{3v}, the vector potential $\mathbf{A}_1$ is rotated by $\pm\frac{2}{3}\pi$ to obtain the other two vector potentials. Then, the total accumulated phases along the nearest-neighbor directions are found to cancel out because of the symmetry of honey-comb lattice. However, the total accumulated phases for the next-nearest-neighbor hopping along the arrowed di-rections of the dashed lines in Fig. 1(a) are just φ. There-fore, the total vector potential and magnetic field can be written as

$$\mathbf{A} = \hbar k_1^L [\sin(2yk_2^L) + \cos(\sqrt{3}xk_2^L)\sin(yk_2^L)]\mathbf{e}_x$$
$$- \sqrt{3}\hbar k_1^L \sin(\sqrt{3}xk_2^L)\cos(yk_2^L)\mathbf{e}_y \qquad (2)$$
$$\mathbf{B} = -2\hbar k_1^L k_2^L [\cos(2yk_2^L) + 2\cos(\sqrt{3}xk_2^L)\cos(yk_2^L)]\mathbf{e}_z.$$

The contours of the magnetic field are plotted in Fig. 1(d). As a consequence, the total Hamiltonian of this cold atomic system can be described by Eq. (1). With Fourier transformation $a_j = \frac{1}{\sqrt{N}}\sum_{\mathbf{k}} e^{i\mathbf{k}\cdot\mathbf{R}_j} a_k$ and $b_j = \frac{1}{\sqrt{N}}\sum_{\mathbf{k}} e^{i\mathbf{k}\cdot\mathbf{R}_j} b_k$, the Hamiltonian of the system can be written by using "spinors" $(a_k, b_k)^t$ as

$$H_k = h_0(\mathbf{k}) + h_1(\mathbf{k})\sigma^1 + h_2(\mathbf{k})\sigma^2 + h_3(\mathbf{k})\sigma^3, \quad (3)$$

where $h_0(\mathbf{k}) = 2t'\cos\varphi\sum_i \cos(\mathbf{k}\cdot\mathbf{a}_i)$, $h_1(\mathbf{k}) = t\sum_i \cos(\mathbf{k}\cdot\mathbf{s}_i)$, $h_2(\mathbf{k}) = t\sum_i \sin(\mathbf{k}\cdot\mathbf{s}_i)$, and $h_3(\mathbf{k}) = M + 2t'\sin\varphi\sum_i \sin(\mathbf{k}\cdot\mathbf{a}_i)$. The vector $h(\mathbf{k}) = [h_1(\mathbf{k}), h_2(\mathbf{k}), h_3(\mathbf{k})]$ is an effective magnetic field of the "spinors." The energy spectra are $E = h_0(\mathbf{k}) \pm |h(\mathbf{k})|$, and the energy gap is $|h_3|$, where $h_3 = h_3(K_+)$ (or $h_3(K_-)$) with $K_\pm = \pm\frac{4\pi}{3a}(1, 0)$. If $h_3 = 0$, the conduction band touches the valence band at two Dirac points K_+ and K_-. The famous TKNN index or Chern number for this system is given by $C = \frac{1}{8\pi}\int_{1BZ} d^2 k \epsilon^{\mu\nu}\hat{h}\cdot(\partial_{k_\mu}\hat{h}\times\partial_{k_\nu}\hat{h})$ [26] with $\hat{h}(\mathbf{k})$ as the unit vector of $h(\mathbf{k})$. It is demonstrated that the gauge invariance C can only take integer values and the quantum Hall conductivity is proportional to the Chern number [4]. For the Haldane's model, different phases of the system can be characterized by different values of C. The phase diagram is depicted in Fig. 2(a) [5], in which the solid line is the critical boundary between the normal insulator with $C = 0$ and the Chern insulator with $C = \pm 1$. It is notable that the phase $\varphi = \pi\tan\theta$ can be controllable by simply choosing the laser angle θ, while the energy difference M between sublattice can be tuned by the phase of laser beams. With such controllability, it is promising to realize the exotic topological phase transition between different Chern numbers in Fig. 2(a).

We now turn to establish a direct connection between the topological Chern number and the atomic density, noting that the latter can be detected with density profile measurements typically used in atomic systems. We first develop a Green's function method to calculate the atomic density. The system is actually described by a Dirac-like Hamiltonian which can be obtained by expanding Eq. (3) around two Dirac points $K_\pm = \pm\frac{4\pi}{3a}(1, 0)$. By the substitution of $\mathbf{k} \to K_\pm + \mathbf{p}$, we have $H_\pm = \mp v_F p_1\sigma^1 - v_F p_2\sigma^2 + m_\pm\sigma^3$ at $K_\pm$, respectively, where $v_F = \frac{\sqrt{3}at}{2}$ is the Fermi velocity and $m_\pm = M \pm 3\sqrt{3}t'\sin\varphi$. Under unitary transformation $\sigma^2 H_-\sigma^2$, we can write the Hamiltonian in a more symmetric form

$$H_\pm = -v_F p_1\sigma^1 - v_F p_2\sigma^2 + m\sigma^3, \quad (4)$$

where the notation $m = \pm m_\pm$ is introduced for simplicity (i.e., we temporally omit subscripts $\pm$ below).

It is observed that the conductivity σ_{xy} (Chern number) of the system is related to the atomic density ρ according to the Streda formula $\sigma_{xy} = \partial\rho/\partial\mathcal{B}|_{\mu,T}$ once an additional uniform magnetic field $\mathcal{B}$ is applied. Such a magnetic field can be simulated by rotating the optical lattice at a constant frequency $\omega = e\mathcal{B}/2m$. We choose the vector potential as
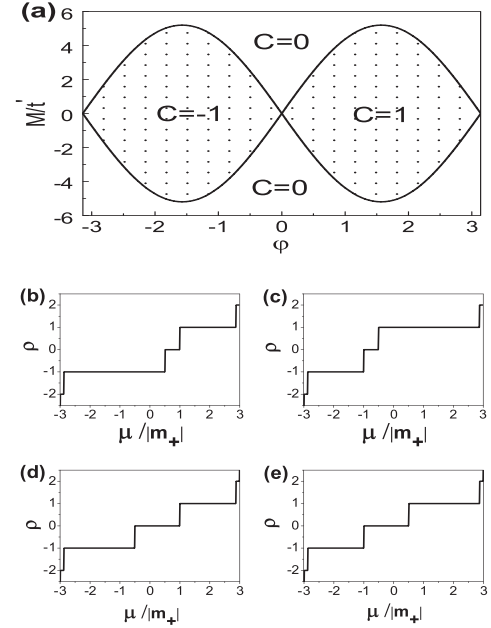

FIG. 2. (a) Phase diagram of the system, where the phase boundary (solid line) corresponds to $h_3 = 0$. (b)–(e) Charge density in units $\mathcal{B}/\phi_0$ for $|m_-| = 0.5|m_+|$ and $e\mathcal{B}\hbar v_F^2 = 4|m_+|$ as a function of normalized chemical potential $\mu/|m_+|$ for four different cases: (b) $m_+ < 0 < m_-$, (c) $m_+ > 0 > m_-$, (d) $m_+ < m_- < 0$, and (e) $m_+ > m_- > 0$.

$\mathcal{A}_0 = \mathcal{A}_1 = 0$ and $\mathcal{A}_2 = \mathcal{B}x$. By using the substitution $\mathbf{p} \to \mathbf{p} + e\mathcal{A}$, Eq. (4) can be solved in the real space. The eigenenergies of the Hamiltonian can be obtained as [5]

$$E_n = \begin{cases} -m\,\text{sgn}(e\mathcal{B}) & n = 0 \\ \pm\sqrt{m^2 + 2n\hbar v_F^2|e\mathcal{B}|} & n = 1, 2, 3\ldots \end{cases}, \quad (5)$$

and the degeneracy of each LL is $|\mathcal{B}/\phi_0|$ per unit area with ϕ_0 the flux quantum. The density ρ in terms of the Green's function for the Dirac Hamiltonian is given by

$$(\slashed{D} + m)G = 1, \qquad \rho = -\text{Tr}[\gamma^0 G(\mathbf{x}, \mathbf{x}')]|_{\mathbf{x}\to\mathbf{x}'} \quad (6)$$

where $\slashed{D} = \gamma^\tau D_\tau$, with $D_0 = \hbar\partial_0 - \mu$, $D_1 = \hbar v_F\partial_1$, $D_2 = \hbar v_F\partial_2 + iev_F\mathcal{B}x$, $\gamma^0 = \sigma^3$, $\gamma^1 = \sigma^2$, and $\gamma^2 = -\sigma^1$ in Euclidean space. From the standard Green function approach, the atomic density is explicitly obtained as

$$\rho_\pm = \left|\frac{\mathcal{B}}{\phi_0}\right|\text{sgn}(\mu)\left\{\text{int}\left[\frac{\mu^2 - m_\pm^2}{2\hbar v_F^2|e\mathcal{B}|}\right] + \frac{1}{2}\right\}\Theta(|\mu| - |m_\pm|)$$
$$\pm\frac{\mathcal{B}}{2\phi_0}\frac{m_\pm}{|m_\pm|}\Theta(|m_\pm| - |\mu|), \quad (7)$$

where Θ stands for the unit step function and int$[x]$ means the largest integer less than x. The second term of Eq. (7) is the atomic density induced into vacuum as $\mu \to 0$ by the uniform magnetic field. It is of parity anomaly since its corresponding Hall current is independent of the magnetic field after multiplying the drift velocity $\mathcal{E}/\mathcal{B}$, where $\mathcal{E}$ is the electric field.

The total atomic density is given by the sum of the densities of the two components $\rho = \rho_+ + \rho_-$. At $\mu = 0$, the Hall conductivity at $\mathcal{B} = 0$ can be obtained from the density by using the Streda formula as $\sigma_{xy} = C\frac{e^2}{h}$, where $C = \frac{1}{2}[\text{sgn}(m_+) - \text{sgn}(m_-)]$ is the Chern number. To show how to detect the Chern number of the system, we consider a finite magnetic field $\mathcal{B}$. The calculated density ρ in unit of $|\mathcal{B}/\phi_0|$ is plotted as a function of the normalized chemical potential $\mu/|m_+|$ (for $|m_-| = 0.5|m_+|$ and $e\hbar v_F^2 \mathcal{B} = 4|m_+|$) in Fig. 2. It is essential that the spatial density profile $\rho(r)$ is uniquely determined by the function $\rho(\mu/|m_+|)$ in the local density approximation, which is typically well satisfied for trapped fermions. Figures 2(b)–2(d) and 2(d) stand for four different cases. The plateaus in the atomic density have one-to-one correspondence to the plateaus in the Hall conductivity due to the finite magnetic field $e\mathcal{B} > 0$. We here focus on $\mu = 0$, which is of our main interest. For $m_+ < 0 < m_-$, which corresponds to $C = -1$, the atomic density $\rho = -\mathcal{B}/\phi_0 < 0$, as shown in Fig. 2(b). For $m_+ > 0 > m_-$, which corresponds to $C = 1$, the density $\rho = \mathcal{B}/\phi_0 > 0$, as shown in Fig. 2(c). For the other two cases $m_+ < m_- < 0$ and $m_+ > m_- > 0$, m_+ and m_- have the same sign, corresponding to $C = 0$, and the density $\rho = 0$, as seen from Figs. 2(d) and 2(e). Therefore, a simple direct relation between the Chern number and the atomic density is established as

$$C = \rho \phi_0 / \mathcal{B}. \tag{8}$$

The important relation (8) actually provides us a feasible way to experimentally detect the Chern number C in different phases. In the absence of $\mathcal{B}$, the density of the cold atoms at $\mu = 0$ is first measured, which is denoted as ρ_0. Then the optical lattice is rotated to generate the effective uniform magnetic field $\mathcal{B}$, and the new density of the cold atoms ρ_1 is measured. If $\rho_1 > \rho_0 (\rho < \rho_0)$, the system is in a Chern insulator phase with Chern number $C = 1 (C = -1)$. If $\rho_1 = \rho_0$, the system behaves like a normal insulator with $C = 0$. Since the density difference is actually quantized in units $\mathcal{B}/\phi_0$, the above method could be rather robust.

Finally, we briefly address an alternative approach to realize the Haldane's QHE. The fermions we discussed are in the s-band of the honeycomb lattice. As for fermions in the p-orbital bands, a Haldane's quantum Hall model without LLs can also be implemented by rotating each optical lattice site around its own center [27].

In summary, we have shown that the Haldane's QHE model can be realized by using ultracold atoms in an optical lattice. We have established a relationship between the Hall conductivity and the equilibrium atomic density, which provides a feasible way to experimentally detect the Chern number C in different phases.

Note added.—Recently, we became aware that a relation between the density profile and the Hall conductivity in conventional QHE was also addressed in Ref. [28]. We thank Dr. H. Zhai for bringing our attention to that work.

*slzhu@scnu.edu.cn
[1] K. V. Klitzing, G. Dorda, and M. Pepper, Phys. Rev. Lett. **45**, 494 (1980).
[2] R. B. Laughlin, Phys. Rev. B **23**, 5632 (1981).
[3] B. I. Halperin, Phys. Rev. B **25**, 2185 (1982).
[4] D. J. Thouless *et al.*, Phys. Rev. Lett. **49**, 405 (1982).
[5] F. D. M. Haldane, Phys. Rev. Lett. **61**, 2015 (1988).
[6] G. W. Semenoff, Phys. Rev. Lett. **53**, 2449 (1984).
[7] S. Deser, R. Jackiw, and S. Templeton, Phys. Rev. Lett. **48**, 975 (1982).
[8] R. Jackiw, Phys. Rev. D **29**, 2375 (1984).
[9] W. A. Bardeen *et al.*, Nucl. Phys. B **218**, 445 (1983).
[10] K. S. Novoselov *et al.*, Nature (London) **438**, 197 (2005).
[11] Y. Zhang *et al.*, Nature (London) **438**, 201 (2005).
[12] J. R. Anglin and W. Ketterle, Nature (London) **416**, 211 (2002).
[13] D. Jaksch *et al.*, Phys. Rev. Lett. **81**, 3108 (1998).
[14] L. M. Duan, E. Demler, and M. D. Lukin, Phys. Rev. Lett. **91**, 090402 (2003).
[15] N. R. Cooper and N. K. Wilkin, Phys. Rev. B **60**, R16279 (1999).
[16] N. K. Wilkin and J. M. F. Gunn, Phys. Rev. Lett. **84**, 6 (2000); T.-L. Ho, *ibid.* **87**, 060403 (2001); T.-L. Ho and C. V. Ciobanu, *ibid.* **85**, 4648 (2000); B. Paredes *et al.*, *ibid.* **87**, 010402 (2001).
[17] A. S. Sorensen, E. Demler, and M. D. Lukin, Phys. Rev. Lett. **94**, 086803 (2005).
[18] R. N. Palmer and D. Jaksch, Phys. Rev. Lett. **96**, 180407 (2006).
[19] S. Viefers, J. Phys. Condens. Matter **20**, 123202 (2008).
[20] N. K. Wilkin, J. M. F. Gunn, and R. A. Smith, Phys. Rev. Lett. **80**, 2265 (1998).
[21] G. Juzeliunas and P. Ohberg, Phys. Rev. Lett. **93**, 033602 (2004); J. Ruseckas *et al.*, *ibid.* **95**, 010404 (2005); Y. Li, C. Bruder, and C. P. Sun, *ibid.* **99**, 130403 (2007).
[22] S. L. Zhu *et al.*, Phys. Rev. Lett. **97**, 240401 (2006).
[23] K. Osterloh *et al.*, Phys. Rev. Lett. **95**, 010403 (2005).
[24] G. Juzeliunas *et al.*, Phys. Rev. A **73**, 025602 (2006).
[25] S. L. Zhu, B. G. Wang, and L. M. Duan, Phys. Rev. Lett. **98**, 260402 (2007).
[26] D. H. Lee, G. M. Zhang, and T. Xiang, Phys. Rev. Lett. **99**, 196805 (2007).
[27] C. Wu, arXiv:0805.3525.
[28] R. O. Umucalilar, H. Zhai, and M. Ö. Oktel, Phys. Rev. Lett. **100**, 070402 (2008).